Cell Reports
Physical Science

CellPress
OPEN ACCESS

Report

Cell membrane buckling governs early-stage ridge formation in butterfly wing scales

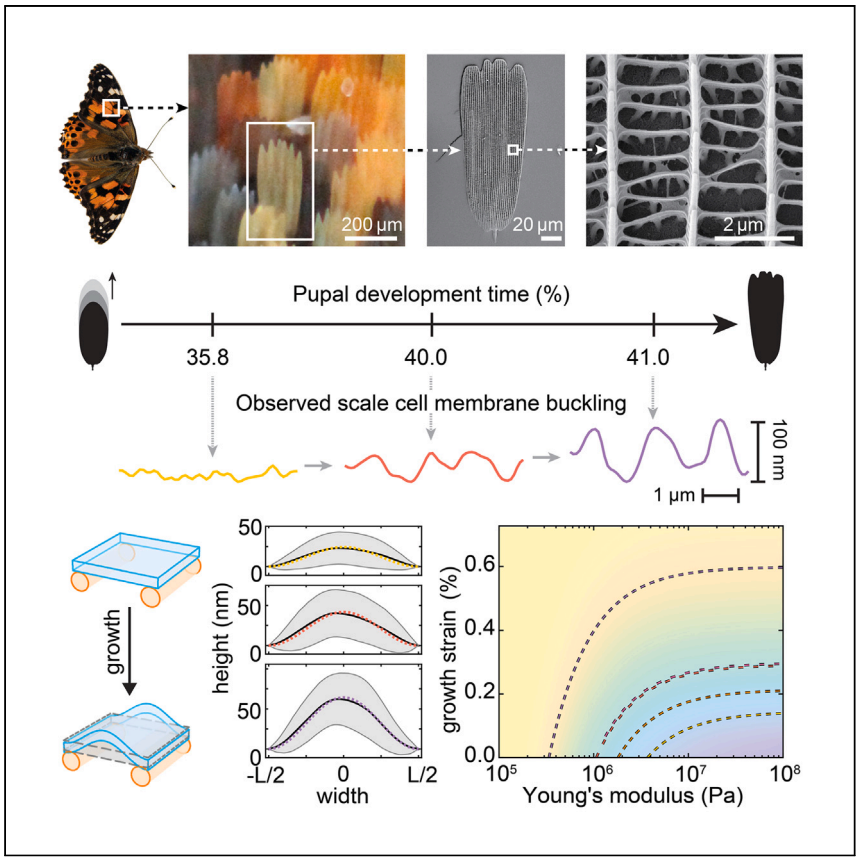

Structurally diverse butterfly wing scale architectures are made from micro- and nanostructured cuticle and are secreted by individual cells during metamorphosis, but the biomechanical processes that enable scale structure formation are not well understood. Here, Totz et al. demonstrate that mechanical buckling initiates the formation of scale ridges.

Jan F. Totz, Anthony D. McDougal, Leonie Wagner, ..., Jörn Dunkel, Bodo D. Wilts, Mathias Kolle

bodo.wilts@plus.ac.at (B.D.W.)
mkolle@mit.edu (M.K.)

Highlights

In vivo phase microscopy of developing scales captures the onset of buckling

Model shows that mechanical buckling instabilities drive initial ridge formation

Actin bundle size and spacing can determine buckling and where ridges form

Totz et al., Cell Reports Physical Science 5, 102063
July 17, 2024
https://doi.org/10.1016/j.xcrp.2024.102063

Please cite this article in press as: Totz et al., Cell membrane buckling governs early-stage ridge formation in butterfly wing scales, Cell Reports Physical Science (2024), https://doi.org/10.1016/j.xcrp.2024.102063

Cell Reports
Physical Science

CellPress
OPEN ACCESS

Report

Cell membrane buckling governs early-stage ridge formation in butterfly wing scales

Jan F. Totz,[1,2,7] Anthony D. McDougal,[1,7] Leonie Wagner,[1,3] Sungsam Kang,[4] Peter T.C. So,[1,4,5] Jörn Dunkel,[2] Bodo D. Wilts,[6,*] and Mathias Kolle[1,8,*]

SUMMARY

During the development of butterfly wing scales, ordered periodic cell membrane modulations occur at the upper surface of scale-forming cells, priming the formation of ridges. Ridges are critical for wing scale functionality, including structural color, wetting characteristics, and thermal performance. Here, we combine a morphoelastic model based on Föppl-von-Kármán plate theory with experimental observations to shed light on the biomechanical processes governing early-stage ridge formation in Painted Lady butterflies. By comparing the model predictions with time-resolved phase imaging data from live butterflies, we provide evidence that the onset of ridge formation is governed by a mechanical buckling transition induced by the interplay of membrane growth and confinement through association with regularly spaced actin bundles. Beyond ridge formation in Painted Lady scales, our theory offers a rationale for the absence of scale ridges in the lower lamina of many lepidopterans and for the alternating ridge pattern of other butterfly species.

INTRODUCTION

Mechanical pattern formation governs the morphogenesis[1,2] of living matter across a wide range of length scales, spanning microbial biofilms,[3] fungi,[4] algae,[5,6] plants,[7,8] and animals.[9–12] Despite biological constraints on available material resources, synthesis processes, and growth conditions, developing organisms can create intricate microscale structures whose complexity remains challenging to replicate with current manufacturing technologies.[13]

The insect order Lepidoptera, encompassing butterflies and moths, offers a particularly fruitful ground for biophysical and biomechanical discovery with potential to inspire design strategies for multifunctional materials.[13,14] The wing scales of many butterfly species are well known to employ photonic crystals to generate striking iridescent colors,[15–17] tailor their wetting characteristics,[18] enable thermal regulation,[19] facilitate sonic cloaking,[20] and improve aerodynamics.[21] Thus far unmatched by synthetic analogs,[13] the remarkable functionality of butterfly wing scales is not only rooted in their material composition but is controlled in large part through material structuring at the nano- and microscale. Yet, although the earliest studies on butterfly scale development date back to the mid-19th century,[22] relatively little is known about the mechanical and physical processes that enable scale formation.

A prominent structural feature found in the wing scales of many butterfly species are the ridges that typically run down the scale's upper surface (Figure 1), whereas the

[1]Department of Mechanical Engineering, Massachusetts Institute of Technology, 77 Massachusetts Avenue, Cambridge, MA 02139, USA

[2]Department of Mathematics, Massachusetts Institute of Technology, 77 Massachusetts Avenue, Cambridge, MA 02139, USA

[3]Department of Informatics, Technical University of Munich, Boltzmannstr. 3, 85748 Garching, Germany

[4]Laser Biomedical Research Center, G. R. Harrison Spectroscopy Laboratory, Massachusetts Institute of Technology, 77 Massachusetts Avenue, Cambridge, MA 02139, USA

[5]Department of Biological Engineering, Massachusetts Institute of Technology, 77 Massachusetts Avenue, Cambridge, MA 02139, USA

[6]Department of Chemistry and Physics of Materials, University of Salzburg, Jakob-Haringer-Str. 2a, 5020 Salzburg, Austria

[7]These authors contributed equally

[8]Lead contact

*Correspondence: bodo.wilts@plus.ac.at (B.D.W.), mkolle@mit.edu (M.K.)

https://doi.org/10.1016/j.xcrp.2024.102063

Please cite this article in press as: Totz et al., Cell membrane buckling governs early-stage ridge formation in butterfly wing scales, Cell Reports Physical Science (2024), https://doi.org/10.1016/j.xcrp.2024.102063

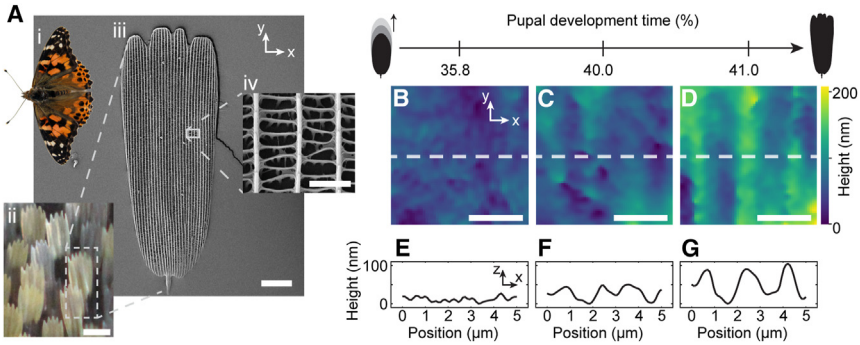

Figure 1. *In vivo* phase data from the surface of young scales shows the early formation of ridges

(A) The wing surfaces of the *V. cardui* butterfly (i) are covered by minute scales (ii), the ultrastructure of which we visualize via scanning electron microscopy (iii). The scales feature prominent ridges that run along the length of the scale on the upper surface (iv).

(B–D) Surface height maps, derived from *in vivo* quantitative phase data of wing scales on a single individual, show the transition from a relatively smooth surface to regular protoridges at 35.8% (B), 40.0% (C), and 41.0% (D) of pupal development.

(E–G) Profiles taken from centerlines in (B)–(D) show the increasing height of the nascent protoridges with increasing pupal development time. Scale bars: (Aii) 200 μm; (Aiii) 20 μm; (Aiv) 2 μm; (B–D) 2 μm.

lower surface is often a flat lamina.[23] The ridges are key contributors to the scale's functionality, as the specialization of the ridge morphology can tune the thermal emissivity,[24] diffractive optics,[15,25,26] and self-cleaning.[27] Ridges have been observed on scales as far back as the Triassic period,[28] indicating that ridges are a robust and reproducible feature of scale cells. How biochemical and biophysical mechanisms jointly determine the formation of ridges still poses many open questions. Several stages and processes are involved in the formation of ridges, including the shaping of the scale cell membrane, the secretion of cuticle, and the shaping of the secreted cuticle through as-of-yet unspecified mechanical processes that involve cuticle sclerotization and hardening.[29–31] In this manuscript, we focus on the very early stages of ridge formation, primarily governed by the shaping of the scale membrane into regular undulations where ridges will form. As previously shown by transmission electron microscopy studies of fixed scale cells,[29,30,32,33] the scale surface begins flat and then deforms into raised wrinkles at regular intervals. At the top of these wrinkles, which we may refer to as "protoridges," cuticle is later secreted and shaped into a stacked lamellae architecture. Although earlier studies of butterfly scales point out various similarities to buckling patterns,[26,34] a detailed mechanical characterization of growing scales is still lacking.

In her seminal 1974 paper, Helen Ghiradella[31] described how, on a single ridge that is already established, the cuticular folds of the lamellae have a periodic spacing that is plausibly consistent with wrinkling of a thin plate. Importantly, while Ghiradella hypothesizes a different buckling event for the initial protoridge—the foundation on which the ridge matures and grows—the mechanical phenomena involved in protoridge formation have yet to be identified and analyzed. A key difficulty in studying the mechanics has lain with the lack of *in vivo* methods to characterize the wing scale cell surface *in situ*. We recently developed a method using quantitative phase imaging to visualize butterfly wing scales *in vivo*[35] and to quantify the localization of membranes in thick animal tissues with nanometer-scale sensitivity.[36] To our knowledge, no other method to date has been demonstrated to record nanoscale height variations of the surface of the wing scales *in vivo* during scale formation. Our imaging approach allows us to observe how the surface morphologies of scale cells change

Please cite this article in press as: Totz et al., Cell membrane buckling governs early-stage ridge formation in butterfly wing scales, Cell Reports Physical Science (2024), https://doi.org/10.1016/j.xcrp.2024.102063

over time within an individual pupa; moreover, our approach leaves the scale cells undisturbed in their natural environment on the developing wing tissue. We thus have a method with which to visualize the earliest moments of protoridge formation and to evaluate the predictions of mechanical models.

Here, we present *in vivo* evidence of the mechanical instability that shapes the butterfly scale's initial surface, which serves as the structural basis for subsequent ridge growth and maturation. We propose a theoretical model based on mechanical buckling that agrees well with the experimental observations.[10] In particular, this model clarifies the role that structural elements, such as actin, play in protoridge growth. Moreover, by analyzing the parameters that drive the buckling of the protoridge, we identify a generic physical mechanism by which butterflies may control early-stage ridge formation.

RESULTS

Mapping evolving profiles of growing protoridges *in vivo* using phase microscopy

Like any other lepidopteran, the Painted Lady butterfly (*Vanessa cardui* L., 1758) grows scales that cover its wings during its pupal stage (Figure 1A). To visualize the growth of scales and the formation of their functional features, we previously developed a method to continuously image growing butterfly wing tissue *in vivo*.[35] To allow optical access to the wing during scale growth, a portion of the pupal case is surgically removed. With speckle-correlation reflection phase microscopy, we can then observe microscopic features with a lateral resolution of $\sim$ 500 nm and detect surface height variations down to about 10 nm, while avoiding photodamage. Finally, we rotate the data volume such that the angled scales are oriented flat.

We focus our observations on the early-stage patterning of the top (abwing) surface of cells forming cover scales on the hindwing, corresponding to the first step in the transformation of a flat membrane to complex cuticular surface modulations that contribute to the scale's functional properties (Figures 1B–1D). After approximately 35%–45% of development (roughly about 3.5–4.5 days) has passed, the flat cell membrane wrinkles to develop into parallel undulations of around 100 nm in height over a time span of about 10 h (Figures 1B–1G).

Prior studies on various species have shown that the ridges form between large actin bundles that also run the length of the scale in an evenly spaced distribution.[37–40] Actin bundles are assemblies of roughly 20–200 individual actin filaments, key components of the cellular cytoskeleton that provides structural integrity to cells. Previous findings indicate that the spacing of this longitudinal structure remains constant during ridge development *in vivo*.[35] Combined with our observations, this suggests that the early stages of ridge formation are characterized by growth of the smooth scale surface between actin bundles to produce a wrinkle or protoridge. To validate this idea, we next formulate and test a biomechanical buckling model that accounts for the combined effects of cell growth and elasticity, actin bundles, and effective cytoplasmic pressure.

A mechanical buckling model for the onset of scale structure formation

We hypothesize that a robust morphoelastic mechanism governs the early-stage evolution of the scale cell topography. As the cell membrane grows, it is constrained by the sub-membrane scaffold of actin bundles (Figures 2A and 2B). This leads to an elastic deformation of the scale cell membrane, which is equivalent to the buckling of a thin plate under biaxial compression.[41] Due to the presence of cytoplasmic

Please cite this article in press as: Totz et al., Cell membrane buckling governs early-stage ridge formation in butterfly wing scales, Cell Reports Physical Science (2024), https://doi.org/10.1016/j.xcrp.2024.102063

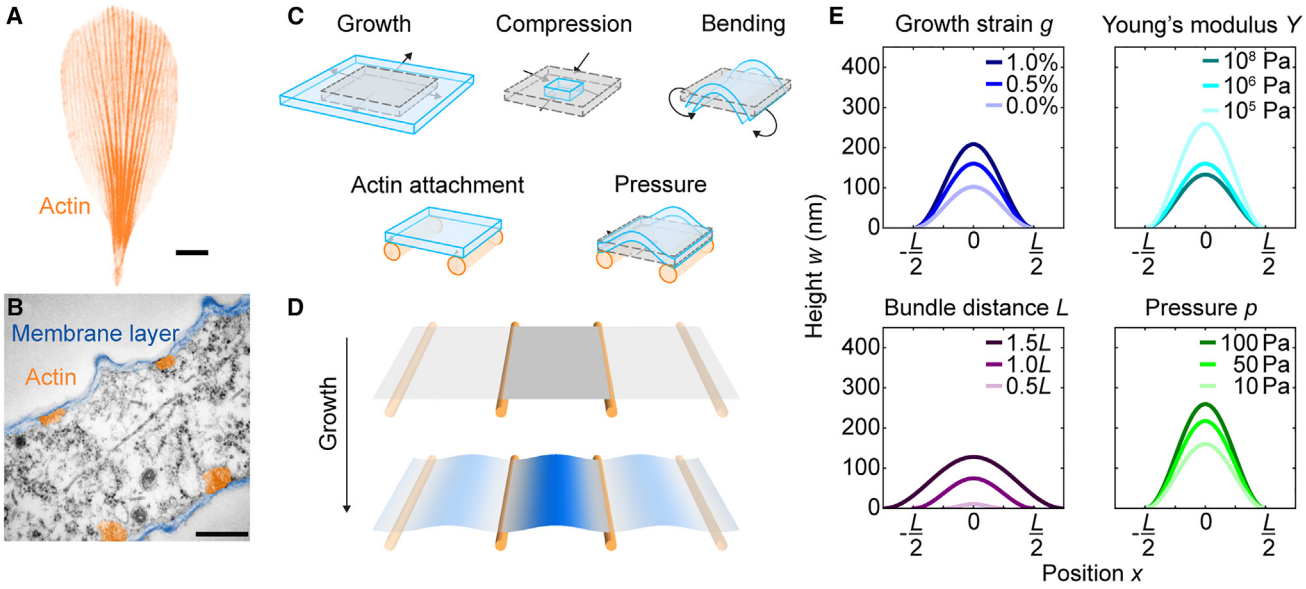

Figure 2. Plate model of constrained growth leads to ridge buckling

(A and B) Relevant biological observables for the model are parallel actin bundles (orange) just within the cell surface (cuticle and membrane, in blue), shown as a projection in (A) and cross-section with the abwing side up in (B); images were adapted under the terms of the CC-BY license from Pomerantz et al.,[33] Copyright 2021, Aaron F. Pomerantz. Blue and orange colors are added to highlight relevant parts of the cross-section.

(C) Growth, compression, bending, actin-membrane coupling, and internal pressure together lead to a buckling transition from a flat to a buckled plate.

(D) Numerical solutions of plate equations (Equations 1 and 2) incorporating the mechanical features shown in (C) demonstrating growth-induced buckling.

(E) Buckling profiles obtained as solutions of the weakly nonlinear Föppl-von-Kármán plate Equations 1 and 2 show the influence of a realistic range of mechanical and geometrical parameters on the buckling amplitude. Model parameters: $\nu = 0.5$, $g = 0.01$, $p = 10$ Pa, $Y = 10^6$ Pa, $h = 20$ nm, and $L = 1.8$ μm. Scale bars: (A) 5 μm; (B) 500 nm.

pressure, the cell membrane buckles outward (Figures 2C and 2D). Here, we consider the basic case where the membrane growth is locally isotropic; our modeling also shows that moderately anisotropic growth conditions also lead to similar buckling deformations.

To test the validity of this hypothesized mechanism, we predict the height of proto-ridges of the buckling cell membrane as a function of Young's modulus Y and growth strain g using classical Föppl-von-Kármán (FvK) plate equations expressed as follows (see Note S2 for the derivation):

$$D\Delta^2 w + hYg\Delta w - h[\chi, w] = p, \qquad \text{(Equation 1)}$$

$$\Delta^2 \chi + YK_G = 0\,. \qquad \text{(Equation 2)}$$

Here, w is the ridge height, χ is the Airy stress potential, which measures the in-plane stress state, $D = \frac{Yh^3}{12(1-\nu^2)}$ is the bending modulus with ν being the Poisson ratio, p is the outward pressure differential between the cell-internal and cell-external spaces, h is the plate thickness, Δ^2 is the biharmonic operator, and $[.,.]$ is the Monge-Ampère bracket operator (see experimental procedures section and Note S2; Equation E6). The growth strain g measures the relative differences $\delta\ell$ between original distances ℓ_o and distances after growth ℓ_g in the plate: $g = \delta\ell/\ell_o$. In Equation 1, which balances out-of-plane stresses acting on the plate, the first term describes the stress due to bending of a flat reference state; the second term is the stress related to the growth-induced prestrain; the third term is the stress due to stretching. All these terms are balanced by a spatially uniform transverse pressure p. Equation 2

Please cite this article in press as: Totz et al., Cell membrane buckling governs early-stage ridge formation in butterfly wing scales, Cell Reports Physical Science (2024), https://doi.org/10.1016/j.xcrp.2024.102063

describes the in-plane stress balance of the plate, whose source term is the Gaussian curvature $K_G = \frac{\partial^2 w}{\partial x^2}\frac{\partial^2 w}{\partial y^2} - \left(\frac{\partial^2 w}{\partial x \partial y}\right)^2$ of the surface.

The periodically spaced actin bundles underneath the scale cell membrane effectively divide the scale surface into repeating parallel domains with comparable growth dynamics; therefore, we focus on a single surface region confined between two actin bundles. Informed by experimental observations of early-stage ridge development (Figure 1) where the measured surface height variation perpendicular to the actin bundles (along x axis) is greater than along the bundle direction (along y axis), we assume that the scale surface profile is constant along the dimension of the actin bundles; this approximation removes the nonlinear terms from the FvK equations, because the Monge-Ampère bracket simplifies to $[\chi, w] = 0$ (see Note S2).

For the interaction between actin bundles and cell membrane, we assume the limiting case of a spatially continuous tight attachment. While previous observations and interpretations provide indications that the actin bundles may have discrete, spatially distributed attachment points on the membrane at later stages of ridge development where chitin secretion has started,[30] in the early stages of the ridge development that are considered here, the assumption of homogeneously tight attachment appears validated by experimental observations of protoridges (Figure 1D). Assuming a tight actin bundle attachment and taking into account the experimentally observed continuous and periodically repeating surface height variations across actin bundles, we therefore impose clamped boundary conditions, $\frac{\partial w}{\partial x} = 0$ and $w = 0$, at the location of the actin bundles.

Using the Rayleigh-Ritz approximation method to compute the maximum amplitude $a = w(x = 0)$, where $x = 0$ marks the location centered between two actin bundles,[42] we can analyze how the protoridge amplitude depends on the relevant mechanical and geometrical parameters (Figure 2E):

$$\frac{g}{g_c} = 1 + \frac{3h^2a^2}{4} - \frac{pL^2}{a\pi^2 Y g_c h^3}. \qquad \text{(Equation 3)}$$

Here, g_c is the critical growth strain for the pressure differential between cell inside and outside being $p = 0$, which is given by

$$g_c = \frac{\pi^2}{3(1-\nu^2)}\left(\frac{h}{L}\right)^2. \qquad \text{(Equation 4)}$$

The amplitude increases with larger growth strains g and larger distances between actin bundles L, since there is more material that can buckle outward. Higher outward pressures p also result in ridges with larger amplitude, a trend that is countered by an increase in membrane stiffness measured by the Young's modulus Y.

We compare our model against the mean *in vivo* protoridge profiles measured experimentally across time for an individual Painted Lady pupa (Figures 3A–3E). For each time point, we manually select surface regions from three to five scales, reconstruct the scale surface height from the phase data, algorithmically segment protoridges as identified by buckled surfaces, and measure profiles along these protoridges (see experimental procedures, Note S1, and Figure S1 for details). To compare these *in vivo* profiles to each other, we normalize their width to a reference length $L = 1.6$ μm and scale the height of the profile by the same normalization factor to facilitate comparison without bias between protoridges. We note that the profile

Please cite this article in press as: Totz et al., Cell membrane buckling governs early-stage ridge formation in butterfly wing scales, Cell Reports Physical Science (2024), https://doi.org/10.1016/j.xcrp.2024.102063

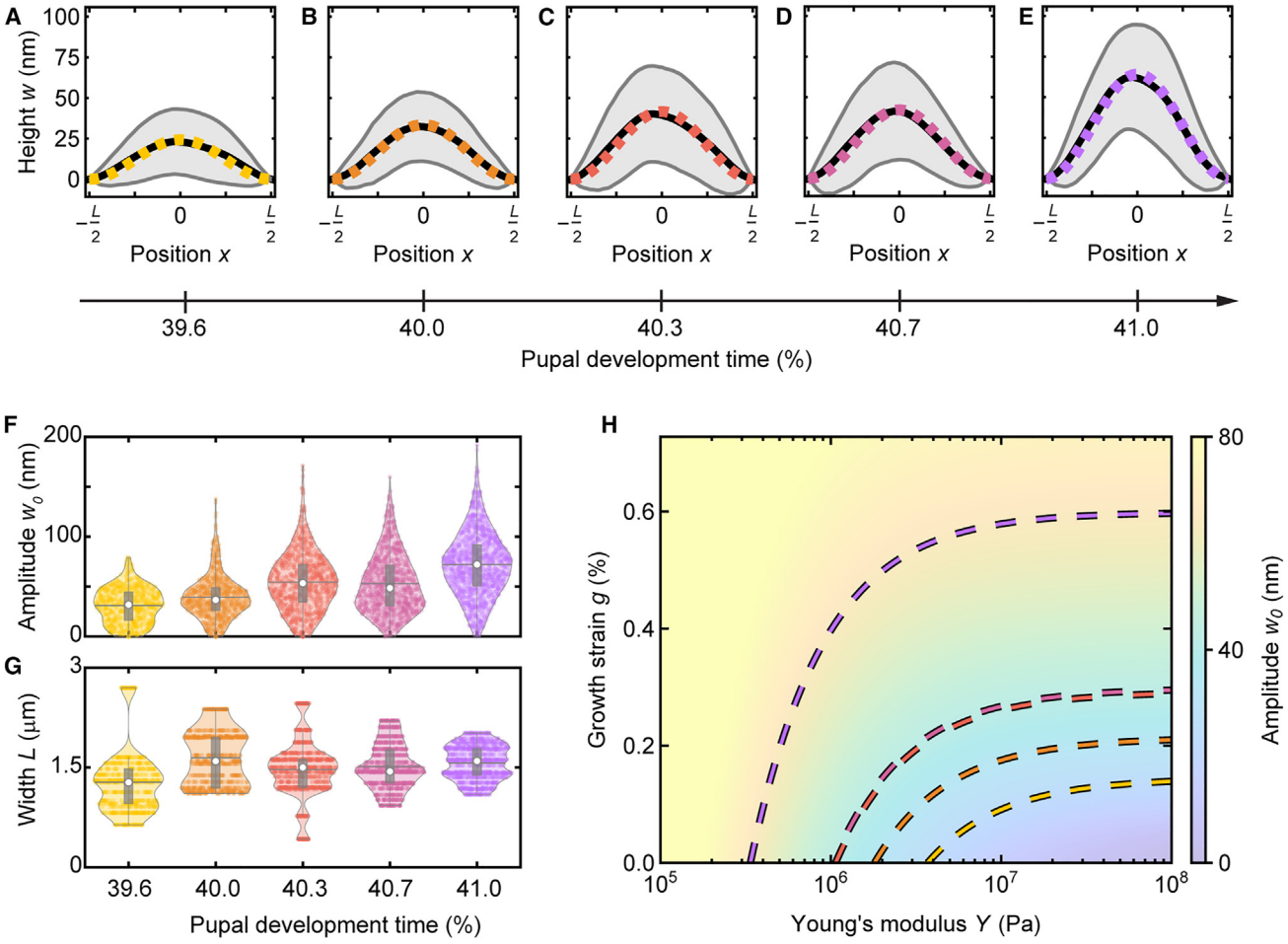

Figure 3. Validation of mechanical buckling hypothesis for early ridge formation

(A–E) Mean values (black) and standard deviation (gray) of *in vivo* height profiles w along position x across the protoridge, matched to predicted height profiles based on the plate mechanics model (dashed curves); height w is scaled with width L of the protoridge (see main text and experimental procedures).

(F) Violin plots of the distribution of *in vivo* protoridge amplitudes w_0, scaled to a reference width of 1.6 μm for morphological comparison against each other and against the simulation, for each time point of development in (A)–(E); shown are the first to third quartile (gray bar), mean (white point), and median (gray line); translucent dots indicate every profile measured at each time point (n = 607, 639, 744, 821, and 911, respectively) for development times 39.6%, 40.0%, 40.3%, 40.6%, and 41.0%.

(G) Violin plots of the distribution of protoridge widths L (unscaled) corresponding to (F).

(H) Phase space of the amplitude w_0 of buckled solutions to numerical simulations for values of Young's modulus Y and growth strain g. Dashed lines show the isocontours that match the amplitudes of the mean profiles in (A)–(E). Note that the curves for 40.3% and 40.7% development time are very closely overlapping. Model parameters: p = 10 Pa, ν = 0.5, h = 20 nm, and bundle distance L = 1.6 μm.

amplitudes for 40.3% development time and 40.7% development time are very similar, and we further note that the 40.7% development time point has data skewed toward smaller profiles. At this time in our surface maps, we observe a transition from somewhat irregular ridges to very regular ridges. This indicates that buckling is not uniform for developmental times earlier than 40.3%, is just beginning to manifest fully at 40.7% development, but soon thereafter becomes regular. To facilitate comparison across 3,722 height profiles, we examine the scaled maximum amplitude, w_0, of each profile measurement and find a gradual increase in protoridge height *in vivo* (Figure 3F). During the observed developmental time span, the mean protoridge widths appear to remain fairly constant and do not vary systematically as the butterfly develops (Figure 3G).

Please cite this article in press as: Totz et al., Cell membrane buckling governs early-stage ridge formation in butterfly wing scales, Cell Reports Physical Science (2024), https://doi.org/10.1016/j.xcrp.2024.102063

When we numerically implement our model with biologically realistic values of Young's modulus Y for soft cuticle ($10^4 - 10^8$ Pa),[43] pressure $p = 10$ Pa, width $L = 1.6\,\mu$m[35], Poisson ratio $\nu = 0.5$, and thickness $h = 20$ nm[30], we find that the theoretical predictions agree well with the experimentally observed profiles in amplitude as well as shape (Figures 3A–3E). We note that the standard deviation of the *in vivo* measurements may pass below zero at the edges, which may be ascribed to biological variability: as the cell membrane grows and the cell develops, it is possible that small fluctuations in pressure locally—which can be considered in physical terms as conservation of the cytoplasmic bulk—induce a secondary deflection inward. Additionally, small material irregularities in the cell membrane, in the cytoplasm, and on the actin bundle or other cellular components are likely to locally perturb the wing surfaces in the *in vivo* experiments.

We can further evaluate the amount of growth strain that realizes the observed buckling amplitude for a given stiffness (Figure 3H). By tracing out the isocurves that correspond to the mean *in vivo* profile amplitudes, our model can predict feasible time courses of Y and g. In addition, we can use the model to place bounds on the material properties of the wing surface. If the stiffness of the scale surface does not decrease (a reasonable assumption, given the increase of cuticle material during scale growth), we find a lower bound of $Y_{min} = 3.5\times10^6$ Pa. Thus, the buckling model is not only supported by our empirical observations but also offers additional insight into the attributes of the forming scale surface.

Rationalizing the early-stage mechanics of ridge formation

A tight association of the scale cell membrane with the underlying actin bundles effectively induces the isolation of the long, thin sections of membrane located between pairs of actin bundles. For each of these membrane sections, isotropic growth leads to first-order buckling; this is substantially more straightforward than controlling higher-order wrinkling instabilities over the entire surface of the scale, which would require the cell membrane's stiffness and bending modulus to be precisely tuned to the factors driving actin bundle spacing, such that the protoridges are aligned between the actin bundles.

One of the functions of the actin bundles appears to be to confine the growing membrane to help shape the wing scale morphology. It has long been documented that actin bundle spacing in the growing scales is closely aligned with the spacing of scale ridges.[37–40] Dinwiddie et al.[39] further demonstrated that inhibition of actin assembly with cytochalasin D prevents scale ridges from properly forming, reasonably prompting the notion that actin bundles somehow drive ridge formation. However, the mechanism by which this happens has not previously been specified. Our morphoelastic model now allows us to propose a mechanism: actin places constraints on the growing cell membrane leading to the creation of ordered membrane buckles, which appears to be the first step in forming scale ridges.

Inter-bundle spacing influences propensity to form protoridges

While the evidence suggests that scale ridges are prepatterned by actin bundles, it is important to consider the regions where the presence of actin bundles does not lead to protoridges. The most widespread example of this can be seen in the lower lamina that comprises the lower surface of many scales; although periodic actin bundles line the lower membrane during development of such scales (Figure 4A, top), protoridges do not form, and the cuticle forms a relatively flat surface.[44,45] An example of that effect is shown in the transmission electron micrograph of a developing scale

Please cite this article in press as: Totz et al., Cell membrane buckling governs early-stage ridge formation in butterfly wing scales, Cell Reports Physical Science (2024), https://doi.org/10.1016/j.xcrp.2024.102063

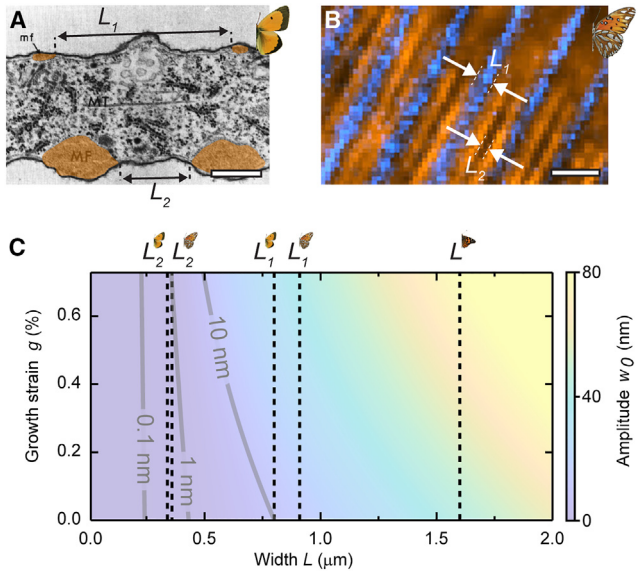

Figure 4. Validation of mechanical buckling hypothesis for early ridge formation

(A) Transmission electron microscopy cross-section of developing scale of *Colias eurytheme*, adapted with permission from Ghiradella,[31] Copyright 1974, John Wiley & Sons; wing image used under the terms of the CC-BY-ND license from Ficarrotta et al.[46] Protoridges form on the upper surface, which has ample spacing L_1 between bundles of actin (also known as microfilaments, indicated by MF); the lower surface, which has significantly smaller spacing between actin bundles L_2, remains flat.

(B) Confocal fluorescence image of the upper surface of a silver wing scale on *Agraulis vanillae*, adapted with permission from Dinwiddie,[39] Copyright 2014, Elsevier. These wing scales only produce protoridges between every other actin bundle; the spacing between actin bundles with protoridges L_1 is larger than the spacing without protoridges L_2.

(C) Phase space of height profiles shows numerical solutions of the scale surface as function of actin bundle spacing L and growth strain g. Black dashed lines indicate actin bundle spacings L from (A) and (B) and Figure 3. For reference, the gray lines correspond to isocontour amplitudes of 0.1 nm, 1 nm, and 10 nm, respectively. Scale bars: (A) 200 nm; (B) 2 μm. Model parameters: p = 10 Pa, ν = 0.5, h = 20 nm, and Y = 1 MPa.

of the Orange Sulphur butterfly *Colias eurytheme* (Figure 4A). Another example for the suppression of protoridges was reported in the silver scales of the Gulf Fritillary butterfly, *Agraulis vanillae*[39]: rather than having a ridge between every pair of actin bundles, every other alternating interstitial region does not form a ridge (Figure 4B). In both cases, the regions devoid of ridges have a smaller distance between actin bundles compared to regions on the same scale where ridges form (Figures 4A and 4B).

How does the interstitial spacing between actin bundles affect ridge formation? Examination of the solution of the FvK equations (Equations 1 and 2) reveals that the buckling transition occurs at a critical growth strain, $g_c \propto L^{-2}$ (Equation 4). Thus, smaller interstitial regions require substantially larger area growth to produce a membrane buckle that forms a protoridge. This effect is illustrated by the results from the mechanical modeling of protoridge formation (Figure 4C).

Figure 4 illustrates two ways that the butterfly may achieve a reduced interstitial spacing to prevent membrane buckling. For the alternating ridge and double actin bundle morphology found in *A. vanillae* scales, the spacing between adjacent actin bundles alternates between a larger value L_1 and a smaller value L_2. In the case of the

Please cite this article in press as: Totz et al., Cell membrane buckling governs early-stage ridge formation in butterfly wing scales, Cell Reports Physical Science (2024), https://doi.org/10.1016/j.xcrp.2024.102063

lower lamina of *Colias eurytheme* scales, the actin bundles are remarkably large, reducing the interstitial space between the bundles. Already Ghiradella noted that it is common to find larger bundles on the lower scale side of the developing cells of many butterfly species.[23] Regardless of the strategy used, a larger spacing (L_1) leads to ridges, while a smaller spacing (L_2) does not yield appreciable ridges. Our model thus suggests that actin bundles not only locate the position of ridges but can also affect whether ridges form or are suppressed based on actin bundle size and distribution.

DISCUSSION

We present quantitative experimental data for the early development of butterfly scale features (Figure 1) and demonstrate with a theoretical model (Figure 2) how a generic instability based on constrained growth leads to robust ordered surface undulations based on the formation of parallel membrane buckles prepatterned by the regular arrangement of actin bundles. The model predictions agree with experimentally measured membrane undulations for biologically realistic model parameters (Figure 3). Furthermore, the theory offers a rationale for the morphology of the lower lamina of the wing scales that is commonly found across Lepidoptera,[47] and explains when ridges do not form on the butterfly wing scale (Figure 4).

Our experimentally validated model provides a starting point for developing more detailed growth models that also take into account the influence of thermal fluctuations,[48] bilayer systems, and the role of enclosing fluid layers or substrates.[49,50] Furthermore, extensions of this model will make it possible to explore higher-order instabilities that lead to serpentine ridges.[51] An important open question not explored here concerns the formation of the actin scaffold, which must require an as-of-yet unknown symmetry-breaking mechanism. While proteins that help organize actin bundles have been identified in the homologous bristle structures in *Drosophila*,[52] further modeling and genetic and proteomic studies are needed to determine the regulation of actin bundling patterning at the early stages of scale and ridge formation in butterflies. An equally intriguing open problem is the formation of ridge multilayers that form during later stages of butterfly wing development.

More generally, the above analysis may provide guidance for investigating topographical surface patterning in other biological systems. Regular parallel surface undulations and patterns are a prominent motif found in bristles, hairs, and scales of flies, butterflies, spiders, and mosquitoes,[33,52–54] on the *C. elegans* body,[55,56] on butterfly eggs,[57] and in flea scales.[58] Often, such structures are formed on the surfaces of single cells and, hence, could rely on actin-constrained formation mechanisms similar to those identified here. Last but not least, due to the generic nature and transferability of elasticity models, the above results may offer insights into how ordered microscale wrinkled structures for engineering applications could be formed with more precision and more scalability than currently achievable with human technology.

EXPERIMENTAL PROCEDURES

Resource availability

Lead contact

Further information and requests for resources and reagents should be directed to and will be fulfilled by the lead contact, Mathias Kolle (mkolle@mit.edu).

Materials availability

This study did not generate new unique materials.

Please cite this article in press as: Totz et al., Cell membrane buckling governs early-stage ridge formation in butterfly wing scales, Cell Reports Physical Science (2024), https://doi.org/10.1016/j.xcrp.2024.102063

Data and code availability

Our data are publicly available on the Zenodo Database: https://doi.org/10.5281/zenodo.8369073.[59] Our code for data processing is available on the Zenodo Database: https://doi.org/10.5281/zenodo.10994275,[60] and the modeling code for plate mechanics is on the Zenodo Database: https://doi.org/10.5281/zenodo.11375797.[61]

Scanning electron microscopy

Scales of butterfly wings were imaged on a Zeiss Gemini Ultra 55 field-emission scanning electron microscope operating at 5 kV, after being covered with a thin gold layer of around 5 nm thickness using a Cressington 108Auto sputter coater to prevent charging.

Live surgery and imaging

We gathered continuous *in vivo* quantitative phase imaging data from a single *V. cardui* pupa throughout almost its entire pupation. Other portions of the resulting dataset related to a broader range of developmental time points, which are not shown here, were previously used in McDougal et al.[35] and made available at Zenodo (Zenodo Data: https://doi.org/10.5281/zenodo.5532941). Briefly, the hindwing tissue is exposed approximately 2 h after the onset of pupation by peeling back the pupal case together with the forewing; the exposed hindwing tissue is then protected with a cover slip, which is sealed to the outer pupal case with dental glue.

After surgery, the pupa's exposed wing is imaged with speckle-correlation reflection phase microscopy, as previously described.[35] The resulting raw interferogram data are processed to yield amplitude and phase information of the butterfly surface, with a lateral resolution of $\sim$ 500 nm and an axial resolution of $\sim$ 1 μm; notably, the phase data quantify surface height variation with a sensitivity of $\sim$ 10 nm.

Phase data analysis

The phase data captured *in vivo* are wrapped on the phase of 2π. For 2D unwrapping (Figures 1B–1D), we first select a region of phase data that shows the scale's surface and then employ the phase unwrapping algorithm from the scikit-image package[62] in Python. For 1D unwrapping (Figures 1E–1G), we extract the phase data along a line and then unwrap that phase profile using the function "unwrap" in MATLAB (MathWorks, Natick MA). The phase of the unwrapped image or line is then converted to height information. Finally, we rotate the height data so that the best-fit plane of the scale surface lies flat.

Plate theory

A detailed derivation of the equations is given in Note S2. The Monge-Ampère bracket is defined as

$$[\chi, w] = \frac{\partial^2 \chi}{\partial x^2}\frac{\partial^2 w}{\partial y^2} + \frac{\partial^2 w}{\partial x^2}\frac{\partial^2 \chi}{\partial y^2} - 2\frac{\partial^2 \chi}{\partial x \partial y}\frac{\partial^2 w}{\partial x \partial y}. \qquad \text{(Equation 5)}$$

Comparison of *in vivo* observed and modeled protoridge data

We use Mathematica 13.1 (Wolfram, Champaign IL) to numerically solve Equation 3, given the parameters in Table S1, for the buckling amplitude a that is plotted in Figures 3H and 4C and to fit the model curves to the experimental data of Figure 3. To quantify the *in vivo* height profiles of Figures 3A–3E, we manually select surface regions from scales at each time point. The phase data from these regions are then unwrapped as described above to derive the height of the scale surface and flatten the region. To segment protoridges from an individual scale surface region, the mean profile of the region is calculated; from this mean profile, the protoridge boundaries are

Cell Reports
Physical Science
Report

determined by the minima surrounding a peak. The entire length of the selected surface region is then cut by these boundaries to select the protoridge. This protoridge is then laid flat, and individual profiles are measured down the length of the protoridge. A common challenge in phase unwrapping is handling phase residues,[63] which can lead to local surface inconsistencies that may affect the analysis. Since perfect linear phase unwrapping assumes that pixel-to-pixel phase does not jump by more than π, we apply a conservative filter for profiles that display a phase jump greater than $3\pi/4$ (191 of 4,074 profiles excluded). To record the height, we then rotate each segmented protoridge so that it lays flat on its own best-fit plane. We further filter out any profile that falls 20 nm below the edge of the segmented region to focus on well-segmented growing surfaces (161 of 3,883 profiles excluded). To comparatively analyze the ridges despite the intrinsic biological variability, we spatially rescale all ridges, so that their actin bundle distances L are normalized.

To specify $L_{1,A}$ and $L_{2,A}$ for use in Figure 4C, we measure the distance between the inner edges of the top and bottom actin bundles shown in Figure 4A.[31] We use the average of four measurements from the original source of Figure 4B[39] to specify each of the values for $L_{1,B}$ and $L_{2,B}$.

SUPPLEMENTAL INFORMATION

Supplemental information can be found online at https://doi.org/10.1016/j.xcrp.2024.102063.

ACKNOWLEDGMENTS

We thank Nicolas Romeo, Ousmane Kodio, Max Thomsen, Hannah Feldstein, Ben H. Miller, and Andrew Blair for helpful discussions and Gerd Schröder-Turk and Doekele Stavenga for feedback on an early draft of this manuscript. This work was supported by a research grant from the Human Frontiers in Science Program (ref.-no: RGP0034/2021 to B.D.W. and M.K.), by the National Science Foundation through the "Designing Materials to Revolutionize and Engineer our Future" program (DMREF-1922321 to M.K), through a Feodor Lynen scholarship from the Humboldt Foundation (to J.F.T.), by a DAAD Rise fellowship (to L.W. and J.F.T.), by the Alfred P. Sloan Foundation under grant G-2021-16758 (J.D.), by the National Institutes of Health (P41EB015871 and R01HL158102 to P.T.C.S. and S.K.), by the MIT MathWorks Professorship Fund (to J.D.), and by Hamamatsu Corporation and Fujikura Ltd. (to P.T.C.S. and S.K.).

AUTHOR CONTRIBUTIONS

J.F.T., A.D.M., B.D.W., and M.K. designed research; J.F.T. and A.D.M. performed research; A.D.M., S.K., P.T.C.S., and M.K. developed the *in vivo* imaging; J.F.T., A.D.M., J.D., B.D.W., and M.K. contributed new reagents/analytic tools; J.F.T., A.D.M., L.W., B.D.W., and M.K. analyzed data; J.F.T., A.D.M., B.D.W., and M.K. wrote the paper; and all authors discussed and reviewed the manuscript.

DECLARATION OF INTERESTS

The authors declare no competing interests.

Received: February 13, 2024
Revised: March 27, 2024
Accepted: June 4, 2024
Published: June 26, 2024

REFERENCES

1. Goriely, A. (2017). The Mathematics and Mechanics of Biological Growth. Interdiscipl. Appl. Math. *45*. https://doi.org/10.1007/978-0-387-87710-5.
2. Hallatschek, O., Datta, S.S., Drescher, K., Dunkel, J., Elgeti, J., Waclaw, B., and Wingreen, N.S. (2023). Proliferating active matter. Nat. Rev. Phys. *5*, 1–13. https://doi.org/10.1038/s42254-023-00593-0.
3. Fei, C., Mao, S., Yan, J., Alert, R., Stone, H.A., Bassler, B.L., Wingreen, N.S., and Košmrlj, A. (2020). Nonuniform growth and surface friction determine bacterial biofilm morphology on soft substrates. Proc. Natl. Acad. Sci. USA *117*, 7622–7632. https://doi.org/10.1073/pnas.1919607117.
4. Money, N.P. (2008). Insights on the mechanics of hyphal growth. Fungal Biol. Rev. *22*, 71–76. https://doi.org/10.1016/j.fbr.2008.05.002.
5. Koehl, M.A.R., Silk, W.K., Liang, H., and Mahadevan, L. (2008). How Kelp Produce Blade Shapes Suited to Different Flow Regimes: A New Wrinkle. Integr. Comp. Biol. *48*, 834–851. https://doi.org/10.1093/icb/icn069.
6. Höhn, S., Honerkamp-Smith, A.R., Haas, P.A., Trong, P.K., and Goldstein, R.E. (2015). Dynamics of a Volvox Embryo Turning Itself Inside Out. Phys. Rev. Lett. *114*, 178101. https://doi.org/10.1103/PhysRevLett.114.178101.
7. Lugo, C.A., Airoldi, C., Chen, C., Crosby, A.J., and Glover, B.J. (2023). Morphoelastic modelling of pattern development in the petal epidermal cell cuticle. J. R. Soc. Interface *20*, 20230001. https://doi.org/10.1098/rsif.2023.0001.
8. Coen, E., and Cosgrove, D.J. (2023). The mechanics of plant morphogenesis. Science *379*, eade8055. https://doi.org/10.1126/science.ade8055.
9. Palmer, M.A., Nerger, B.A., Goodwin, K., Sudhakar, A., Lemke, S.B., Ravindran, P.T., Toettcher, J.E., Košmrlj, A., and Nelson, C.M. (2021). Stress Ball Morphogenesis: How the Lizard Builds Its Lung. Sci. Adv. *7*, eabk0161. https://doi.org/10.1126/sciadv.abk0161.
10. Audoly, B., and Pomeau, Y. (2010). Elasticity and Geometry: From Hair Curls to the Non-linear Response of Shells (Oxford University Press).
11. Chirat, R., Moulton, D.E., and Goriely, A. (2013). Mechanical Basis of Morphogenesis and Convergent Evolution of Spiny Seashells. Proc. Natl. Acad. Sci. USA *110*, 6015–6020. https://doi.org/10.1073/pnas.1220443110.
12. Lee, J.-H., Park, H.S., and Holmes, D.P. (2021). Elastic Instabilities Govern the Morphogenesis of the Optic Cup. Phys. Rev. Lett. *127*, 138102. https://doi.org/10.1103/PhysRevLett.127.138102.
13. McDougal, A., Miller, B., Singh, M., and Kolle, M. (2019). Biological Growth and Synthetic Fabrication of Structurally Colored Materials. J. Opt. *21*, 073001. https://doi.org/10.1088/2040-8986/aaff39.
14. Schroeder, T.B.H., Houghtaling, J., Wilts, B.D., and Mayer, M. (2018). It's Not a Bug, It's a Feature: Functional Materials in Insects. Adv. Mater. *30*, 1705322. https://doi.org/10.1002/adma.201705322.
15. Smith, G.S. (2009). Structural Color of Morpho Butterflies. Am. J. Phys. *77*, 1010–1019. https://doi.org/10.1119/1.3192768.
16. Wilts, B.D., Apeleo Zubiri, B., Klatt, M.A., Butz, B., Fischer, M.G., Kelly, S.T., Spiecker, E., Steiner, U., and Schröder-Turk, G.E. (2017). Butterfly gyroid nanostructures as a time-frozen glimpse of intracellular membrane development. Sci. Adv. *3*, e1603119. https://doi.org/10.1126/sciadv.1603119.
17. Kinoshita, S. (2008). Structural Colors in the Realm of Nature. World Scientific. https://www.worldscientific.com/worldscibooks/10.1142/6496#t=aboutBook.
18. Bixler, G.D., and Bhushan, B. (2014). Rice- and Butterfly-Wing Effect Inspired Self- Cleaning and Low Drag Micro/Nanopatterned Surfaces in Water, Oil, and Air Flow. Nanoscale *6*, 76–96. https://doi.org/10.1039/c3nr04755e.
19. Pris, A.D., Utturkar, Y., Surman, C., Morris, W.G., Vert, A., Zalyubovskiy, S., Deng, T., Ghiradella, H.T., and Potyrailo, R.A. (2012). Towards High-Speed Imaging of Infrared Photons with Bio-Inspired Nanoarchitectures. Nat. Photonics *6*, 195–200. https://doi.org/10.1038/nphoton.2011.355.
20. Shen, Z., Neil, T.R., Robert, D., Drinkwater, B.W., and Holderied, M.W. (2018). Biomechanics of a Moth Scale at Ultrasonic Frequencies. Proc. Natl. Acad. Sci. USA *115*, 12200–12205. https://doi.org/10.1073/pnas.1810025115.
21. Slegers, N., Heilman, M., Cranford, J., Lang, A., Yoder, J., and Habegger, M.L. (2017). Beneficial Aerodynamic Effect of Wing Scales on the Climbing Flight of Butterflies. Bioinspiration Biomimetics *12*, 016013. https://doi.org/10.1088/1748-3190/aa551d.
22. Semper, C. (1857). Über Die Bildung Der Flügel, Schuppen Und Haare Bei Den Lepidopteren. Z. Wiss. Zool. *8*, 326–339.
23. Ghiradella, H. (2010). Insect Cuticular Surface Modifications. Adv. Insect Physiol *38*, 135–180. https://doi.org/10.1016/s0065-2806(10)38006-4.
24. Krishna, A., Nie, X., Warren, A.D., Llorente-Bousquets, J.E., Briscoe, A.D., and Lee, J. (2020). Infrared Optical and Thermal Properties of Microstructures in Butterfly Wings. Proc. Natl. Acad. Sci. USA *117*, 1566–1572. https://doi.org/10.1073/pnas.1906356117.
25. Vukusic, P., Sambles, J.R., Lawrence, C.R., and Wootton, R.J. (1999). Quantified Interference and Diffraction in Single Morpho Butterfly Scales. Proc. R. Soc. A B *266*, 1403–1411. https://doi.org/10.1098/rspb.1999.0794.
26. Wilts, B.D., Giraldo, M.A., and Stavenga, D.G. (2016). Unique Wing Scale Photonics of Male Rajah Brooke's Birdwing Butterflies. Front. Zool. *13*, 36. https://doi.org/10.1186/s12983-016-0168-7.
27. Köchling, P., Niebel, A., Hurka, K., Vorholt, F., and Hölscher, H. (2020). On the Multifunctionality of Butterfly Scales: A Scaling Law for the Ridges of Cover Scales. Faraday Discuss *223*, 195–206. https://doi.org/10.1039/d0fd00038h.
28. van Eldijk, T.J.B., Wappler, T., Strother, P.K., van der Weijst, C.M.H., Rajaei, H., Visscher, H., and van de Schootbrugge, B. (2018). A Triassic-Jurassic Window into the Evolution of Lepidoptera. Sci. Adv. *4*, e1701568. https://doi.org/10.1126/sciadv.1701568.
29. Paweletz, N., and Schlote, F.-W. (1964). Die Entwicklung der Schmetterlingsschuppe bei Ephestia kühniella Zeller. Z. Zellforsch *63*, 840–870. https://doi.org/10.1007/bf00336225.
30. Greenstein, M.E. (1972). The Ultrastructure of Developing Wings in the Giant Silkmoth, Hyalophora Cecropia. II. Scale-forming and Socket-Forming Cells. J. Morphol. *136*, 23–51. https://doi.org/10.1002/jmor.1051360103.
31. Ghiradella, H. (1974). Development of Ultraviolet-Reflecting Butterfly Scales: How to Make an Interference Filter. J. Morphol. *142*, 395–409. https://doi.org/10.1002/jmor.1051420404.
32. Ghiradella, H. (1991). Light and Color on the Wing: Structural Colors in Butterflies and Moths. Appl. Opt. *30*, 3492–3500. https://doi.org/10.1364/AO.30.003492.
33. Pomerantz, A.F., Siddique, R.H., Cash, E.I., Kishi, Y., Pinna, C., Hammar, K., Gomez, D., Elias, M., and Patel, N.H. (2021). Developmental, Cellular and Biochemical Basis of Transparency in Clearwing Butterflies. J. Exp. Biol. *224*, jeb237917. https://doi.org/10.1242/jeb.237917.
34. Parnell, A.J., Bradford, J.E., Curran, E.V., Washington, A.L., Adams, G., Brien, M.N., Burg, S.L., Morochz, C., Fairclough, J.P.A., Vukusic, P., et al. (2018). Wing Scale Ultrastructure Underlying Convergent and Divergent Iridescent Colours in Mimetic Heliconius Butterflies. J. R. Soc. Interface *15*, 20170948. https://doi.org/10.1098/rsif.2017.0948.
35. McDougal, A.D., Kang, S., Yaqoob, Z., So, P.T.C., and Kolle, M. (2021). In Vivo Visualization of Butterfly Scale Cell Morphogenesis in Vanessa Cardui. Proc. Natl. Acad. Sci. USA *118*, e2112009118. https://doi.org/10.1073/pnas.2112009118.
36. Kang, S., Zhou, R., Brelen, M., Mak, H.K., Lin, Y., So, P.T.C., and Yaqoob, Z. (2023). Mapping nanoscale topographic features in thick tissues with speckle diffraction tomography. Light Sci. Appl. *12*, 200. https://doi.org/10.1038/s41377-023-01240-0.
37. Picken, L.E.R. (1949). Shape and Molecular Orientation in Lepidopteran Scales. Phil. Trans. R. Soc. B *234*, 1–28. https://doi.org/10.1098/rstb.1949.0005.
38. Overton, J. (1966). Microtubules and Microfibrils in Morphogenesis of the Scale Cells of Ephestia Kühniella. J. Cell Biol. *29*, 293–305. https://doi.org/10.1083/jcb.29.2.293.
39. Dinwiddie, A., Null, R., Pizzano, M., Chuong, L., Leigh Krup, A., Ee Tan, H., and Patel, N.H. (2014). Dynamics of F-actin Prefigure the Structure of Butterfly Wing Scales. Dev. Biol.

392, 404–418. https://doi.org/10.1016/j.ydbio.2014.06.005.

40. Day, C.R., Hanly, J.J., Ren, A., and Martin, A. (2019). Sub-Micrometer Insights into the Cytoskeletal Dynamics and Ultrastructural Diversity of Butterfly Wing Scales. Dev. Dynam. *248*, 657–670. https://doi.org/10.1002/dvdy.63.

41. Audoly, B., Roman, B., and Pocheau, A. (2002). Secondary Buckling Patterns of a Thin Plate under In-Plane Compression. Eur. Phys. J. B *27*, 7–10. https://doi.org/10.1140/epjb/e20020124.

42. Wu, B., and Yu, Y. (2014). A Simplified Analysis on Buckling of Stressed and Pressurized Thin Films on Substrates. Arch. Appl. Mech. *84*, 149–157. https://doi.org/10.1007/s00419- 013-0790-1.

43. Vincent, J.F.V., and Wegst, U.G.K. (2004). Design and Mechanical Properties of Insect Cuticle. Arthropod Struct. Dev. *33*, 187–199. https://doi.org/10.1016/j.asd.2004.05.006.

44. Thayer, R.C., Allen, F.I., and Patel, N.H. (2020). Structural Color in Junonia Butterflies Evolves by Tuning Scale Lamina Thickness. D. Tautz, C. Desplan, and C. Jiggins, eds. *9*, e52187. https://doi.org/10.7554/eLife.52187.

45. Stavenga, D.G., Leertouwer, H.L., and Wilts, B.D. (2014). Coloration Principles of Nymphaline Butterflies – Thin Films, Melanin, Ommochromes and Wing Scale Stacking. J. Exp. Biol. *217*, 2171–2180. https://doi.org/10.1242/jeb.098673.

46. Ficarrotta, V., Hanly, J.J., Loh, L.S., Francescutti, C.M., Ren, A., Tunström, K., Wheat, C.W., Porter, A.H., Counterman, B.A., and Martin, A. (2022). A Genetic Switch for Male UV Iridescence in an Incipient Species Pair of Sulphur Butterflies. Proc. Natl. Acad. Sci. USA *119*, e2109255118. https://doi.org/10.1073/pnas.2109255118.

47. Stavenga, D.G. (2014). Thin film and multilayer optics cause structural colors of many insects and birds. Mater. Today Proc. *1*, 109–121. https://doi.org/10.1016/j.matpr.2014. 09.007.

48. Morshedifard, A., Ruiz-García, M., Abdolhosseini Qomi, M.J., and Košmrlj, A. (2021). Buckling of Thermalized Elastic Sheets. J. Mech. Phys. Solid. *149*, 104296. https://doi.org/10.1016/j.jmps.2021.104296.

49. King, H., Schroll, R.D., Davidovitch, B., and Menon, N. (2012). Elastic Sheet on a Liquid Drop Reveals Wrinkling and Crumpling as Distinct Symmetry-Breaking Instabilities. Proc. Natl. Acad. Sci. USA *109*, 9716–9720. https://doi.org/10.1073/pnas.1201201109.

50. Oshri, O., Brau, F., and Diamant, H. (2015). Wrinkles and Folds in a Fluid-Supported Sheet of Finite Size. Phys. Rev. E *91*, 052408. https://doi.org/10.1103/PhysRevE.91.052408.

51. Ingram, A.L., and Parker, A.R. (2008). A review of the diversity and evolution of photonic structures in butterflies, incorporating the work of John Huxley (The Natural History Museum, London from 1961 to 1990). Phil. Trans. R. Soc. B *363*, 2465–2480. https://doi.org/10.1098/rstb.2007.2258.

52. Tilney, L.G., and DeRosier, D.J. (2005). How to Make a Curved Drosophila Bristle Using Straight Actin Bundles. Proc. Natl. Acad. Sci. USA *102*, 18785–18792. https://doi.org/10.1073/pnas.0509437102.

53. Djokic, S., Bakhrat, A., Tsurim, I., Urakova, N., Rasgon, J.L., and Abdu, U. (2020). Actin Bundles Play a Different Role in Shaping Scales Compared to Bristles in the Mosquito Aedes Aegypti. Sci. Rep. *10*, 14885. https://doi.org/10.1038/s41598-020-71911-0.

54. Wilts, B.D., Otto, J., and Stavenga, D.G. (2020). Ultra-dense, curved, grating optics determines peacock spider coloration. Nanoscale Adv. *2*, 1122–1127. https://doi.org/10.1039/C9NA00494G.

55. Priess, J.R., and Hirsh, D.I. (1986). Caenorhabditis Elegans Morphogenesis: The Role of the Cytoskeleton in Elongation of the Embryo. Dev. Biol. *117*, 156–173. https://doi.org/10.1016/0012-1606(86)90358-1.

56. Costa, M., Draper, B.W., and Priess, J.R. (1997). The Role of Actin Filaments in Patterning the Caenorhabditis Elegans Cuticle. Dev. Biol. *184*, 373–384. https://doi.org/10.1006/dbio.1997.8530.

57. Peterson, A. (1970). Eggs from Miscellaneous Species of Rhopalocera-Lepidoptera. Fla. Entomol. *53*, 65–71. https://doi.org/10.2307/3493448.

58. Vanthournout, B., Rousaki, A., Parmentier, T., Janssens, F., Mertens, J., Vandenabeele, P., D'Alba, L., and Shawkey, M. (2021). Springtail Coloration at a Finer Scale: Mechanisms behind Vibrant Collembolan Metallic Colours. J. R. Soc. Interface *18*, 20210188. https://doi.org/10.1098/rsif.2021.0188.

59. Totz, J.F., McDougal, A.D., Wagner, L., Kang, S., So, P.T., Dunkel, J., Wilts, B.D., and Kolle, M. (2024a). Cell Membrane Buckling Governs Early-Stage Ridge Formation in Butterfly Wing Scales: Data (Zenodo). https://doi.org/10.5281/zenodo.8369073.

60. (2024). Cell Membrane Buckling Governs Early-Stage Ridge Formation in Butterfly Wing Scales: Analysis (Zenodo). https://doi.org/10.5281/zenodo.10994275.

61. (2024). Cell Membrane Buckling Governs Early-Stage Ridge Formation in Butterfly Wing Scales: Plate Equations (Zenodo). https://doi.org/10.5281/zenodo.11375797.

62. van der Walt, S., Schönberger, J.L., Nunez-Iglesias, J., Boulogne, F., Warner, J.D., Yager, N., Gouillart, E., and Yu, T.; scikit-image contributors (2014). Scikit-Image: Image Processing in Python. PeerJ *2*, e453. https://doi.org/10.7717/peerj.453.

63. Goldstein, R.M., Zebker, H.A., and Werner, C.L. (1988). Satellite Radar Interferometry: Two-dimensional Phase Unwrapping. Radio Sci. *23*, 713–720. https://doi.org/10.1029/RS023i004p00713.